Progress In Electromagnetics Research C, Vol. 14, 185–195, 2010

A STACKED MICROSTRIP PATCH ANTENNA WITH FRACTAL SHAPED DEFECTS

H. Tiwari and M. V. Kartikeyan

Department of Electronics and Computer Engineering
Indian Institute of Technology
Roorkee 247667, India

Abstract—In this paper, a novel type of stacked microstrip patch antenna is presented in which fractal shaped defects have been excoriated from the patch surfaces. The antenna has been designed for dual band operation at the WLAN 2.4 GHz and 5.8 GHz frequency bands and size reduction for both the stacked patches is achieved due to the use of fractal shaped defects. The antenna was simulated using CST Microwave Studio 2010 and optimized using Particle Swarm Optimization (inbuilt in CST). The fabricated antenna's measurement results were found to be in good agreement with the simulated results.

1. INTRODUCTION

Microstrip antennas are very popular due to their properties, such as low profile, low cost, conformability and ease of integration with active devices. Because of the need to integrate these antennas in MMIC circuits and also their use in other wireless communication applications the size of these microstrip antennas should be as small as possible without compromising on their performance. Many techniques which have been used for antenna miniaturization, such as i) use of high permittivity substrates [1], ii) applying resistive or reactive loading [2], iii) increasing the electrical length of antenna [3], iv) use of notches and short circuits on the patch antenna [4], v) use of magnetic substrates etc. have been quoted in [5] and [6]. Various shapes of slots and slits have been embedded on patch antennas to reduce their size. Recently a microstrip antenna with Koch shaped fractal defects was presented [6] in which 85% size reduction was achieved.

Corresponding author: M. V. Kartikeyan (kartkfec@iitr.ernet.in).

Various techniques also exist for dual banding of microstrip antennas [7–9]. In this paper, a stacked microstrip patch antenna with fractal shaped defects is presented for dual band operation. The introduction of a stacked patch along with the dimensionalities associated with multiple fractal defects provide us with a large number of parameters to optimize the dual band behavior of the antenna. A stacked patch antenna with U-slots for similar dual-band operation was designed by the authors earlier [10]. In comparison, the antenna in this paper obtains a size reduction of around 67% for both the patches.

2. ANTENNA GEOMETRY

The antenna configuration for the bottom/fed and top/parasitic patches is shown in Figure 1. Four Koch shaped fractal defects are symmetrically excoriated from both the top and bottom patch surfaces. The substrate used has relative permittivity $\varepsilon_r = 3.38$ and thickness 1.524 mm (60 mil). The antenna is fed via a probe in the bottom patch at a distance of $xo = 3.2$ mm from the radiating edge (Figure 1(b)). The gap between the two substrates is $ha = 8$ mm and the parasitic

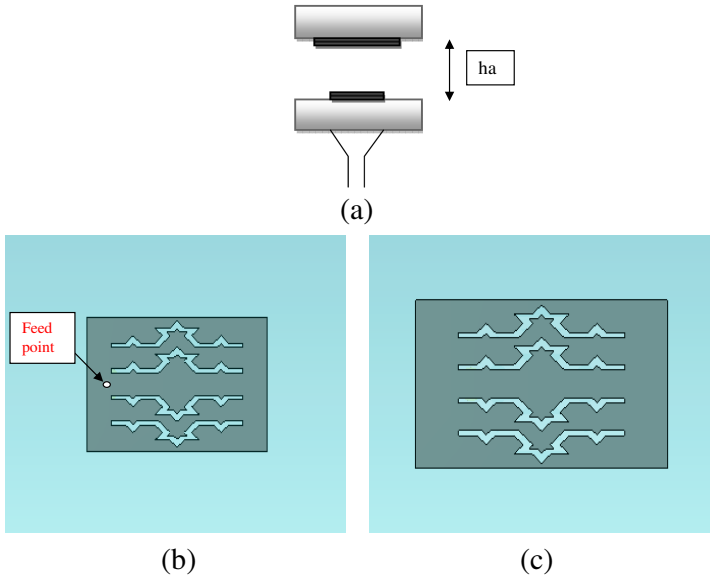

Figure 1. (a) Stack antenna configuration. (b) & (c) The bottom and top patches (with $ha = 8$ mm air gap between the substrates on which they are etched).

patch is etched on the bottom side of the upper substrate. The size of the substrate used is 6 cm by 6 cm. The size of the bottom patch is $pl \times pw = 29.1 \times 18.584$ mm, and size of the top patch is $pl2 \times pw2 = 40.1 \times 23.12$ mm. For the symmetrical fractal shaped defects on the bottom patch the length is $fl = 21.3$ mm and their thickness is $ft = 0.55$ mm. The defects nearest to the centre are placed at an offset of $fo = 2.13$ mm from the centre while defects on either side of the centre are placed at a distance of $fd = 3.55$ mm from each other. The corresponding dimensions for the parasitic patch are $fl2 = 26.5$ mm, $ft2 = 0.69$ mm, $fo2 = 2.65$ mm and $fd2 = 4.417$ mm. The stacked U-slot antenna in [10] had its lower and upper patches of dimensions 41.9×39.9 mm and 53.4×53.4 mm respectively for dual band operation at similar frequency bands. Hence, with the use of fractal-slots size reduction of roughly 67% is obtained for both the patches.

So initially the total number of dimensions for optimizing the dual band performance of the antenna are 14, namely, $pl, pl2, pw, pw2, fl, fl2, ft, ft2, fo, fo2, fd, fd2, ha$ and xo. These were the dimensions which were used in optimizing the antenna. For optimization PSO algorithm inbuilt in CST Microwave Studio 2010 was used.

3. RETURN LOSS AND PARAMETRIC VARIATIONS

The simulated and fabricated return loss results are shown in Figures 2 and 3. The antenna covers the WLAN standards IEEE 802.11 b (2.4 GHz band) and IEEE 82.11 a (5.8 GHz band). The simulated bandwidth at the 2.4 GHz band is around 120 MHz and at the 5.8 GHz band is around 160 MHz. After fabrication the return loss of the

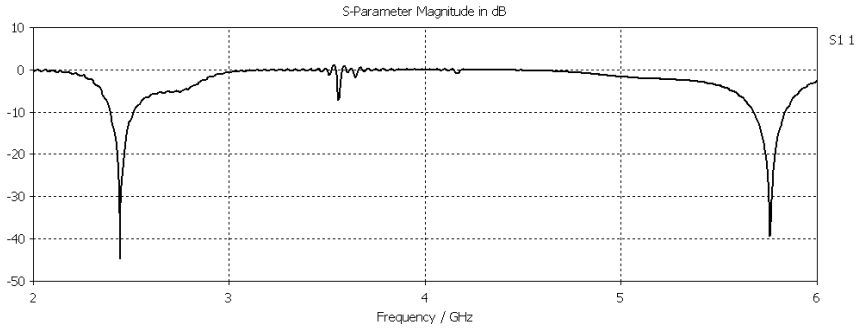

Figure 2. The simulated return loss of the antenna.

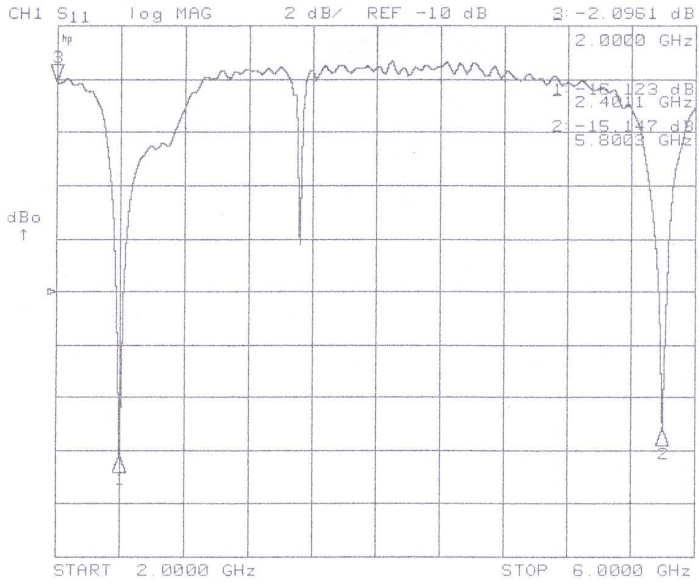

Figure 3. The fabricated return loss of the antenna.

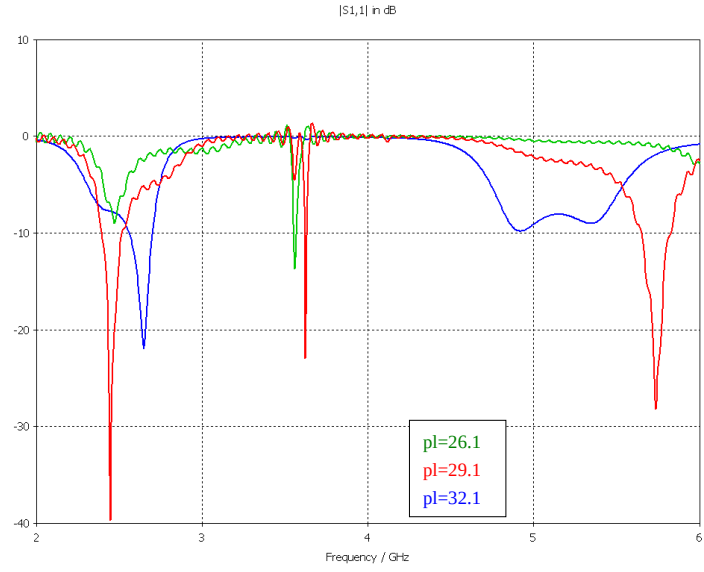

Figure 4. Effect of varying *pl* on the return loss pattern.

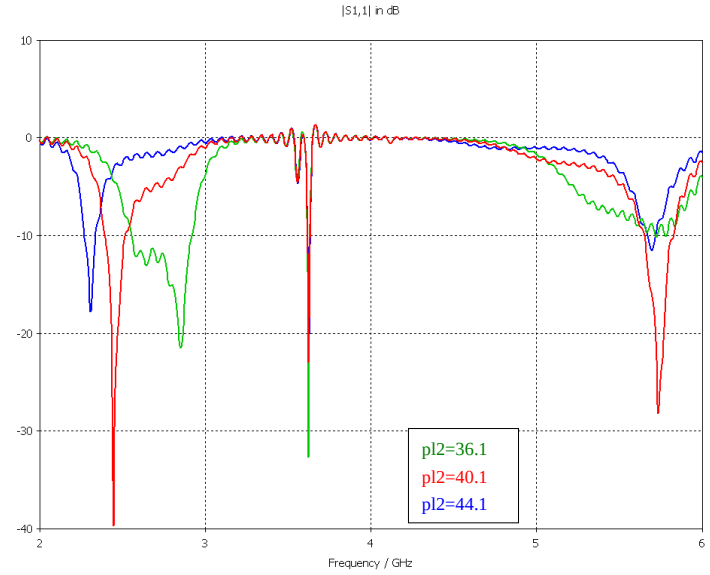

Figure 5. Effect of varying $pl2$ on the return loss pattern.

antenna was tested on HP Network Analyzer and the fabricated result was found to be in good agreement with the simulated result.

After performing parametric variations and the optimization using PSO the dimensions which were influencing the return loss of the antenna most strongly were found to be $pl, pl2, fl, fl2$ and ha. The results of varying these parameters on the return loss behavior of the antenna are shown in the Figures 4 through 8. Varying the bottom patch length pl influences both the resonant frequencies which shows that it is the most important design parameter. The upper patch length $pl2$ controls the level of the second resonance and the position of the first resonance. Varying the length of the fractal defect on the bottom patch fl has a significant influence on the deepness of the second resonance. The length of the fractal defect on the parasitic patch has a slight influence on the position of the second resonance. The air gap between the two patches which controls the electromagnetic coupling between them is responsible for the position of the second resonance.

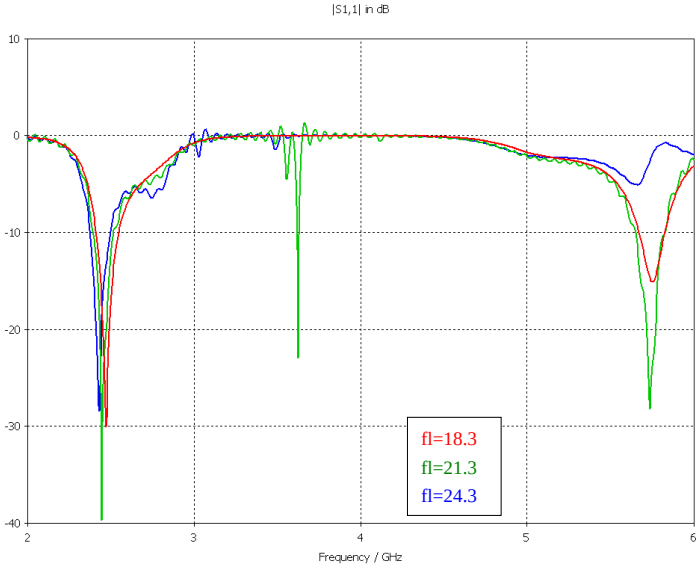

Figure 6. Effect of varying fl on the return loss pattern.

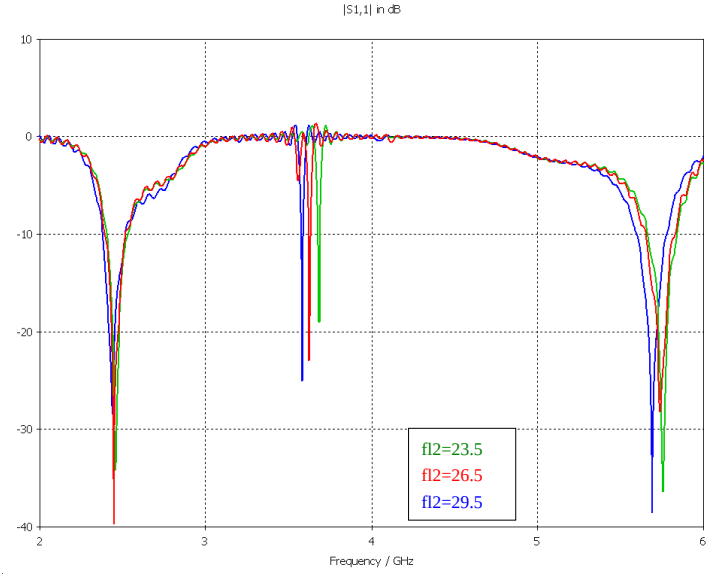

Figure 7. Effect of varying $fl2$ on the return loss pattern.

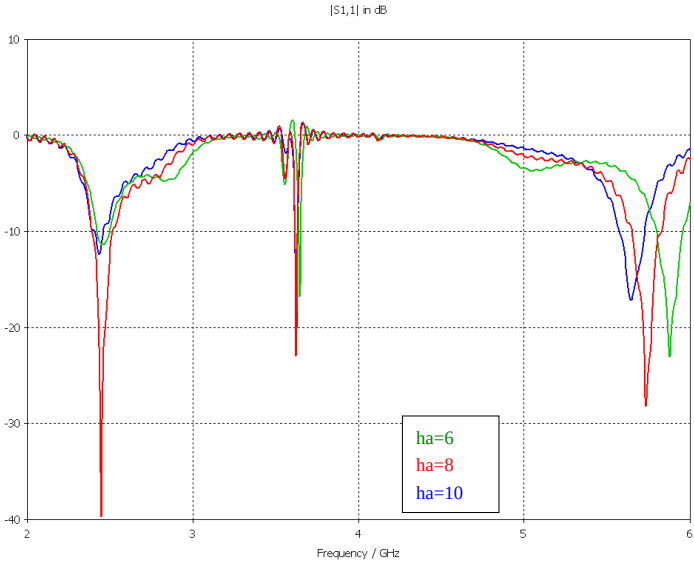

Figure 8. Effect of varying *ha* on the return loss pattern.

4. CURRENT DISTRIBUTION

The current distributions for the lower and upper patches at the 2.4 GHz and 5.8 GHz bands are shown in Figures 9 and 10. As in [6], it can be seen that the current paths have been lengthened because of the introduction of Koch-shaped fractal defects on both the patches which leads to an increase in electrical length and hence a decrease in

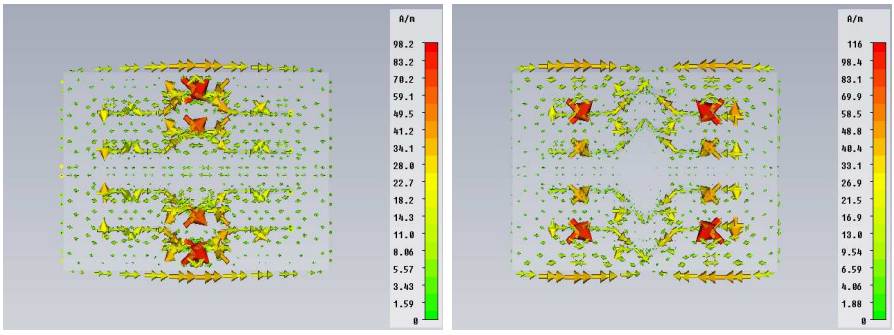

Figure 9. Current distribution on bottom patch at 2.4 GHz and 5.8 GHz bands.

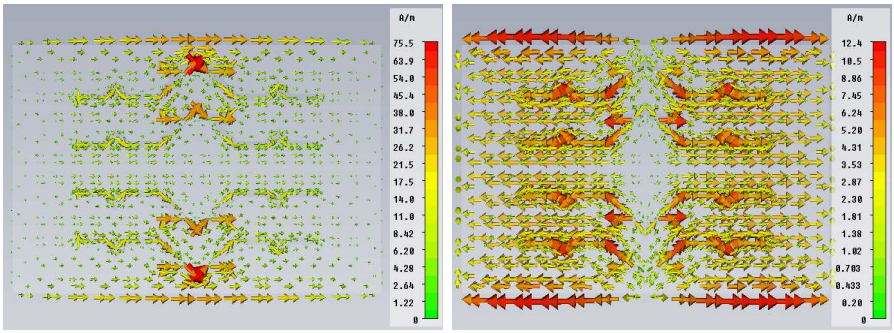

Figure 10. Current distribution on upper patch at 2.4 GHz and 5.8 GHz bands.

Figure 11. The fabricated antenna being tested on a network analyzer.

overall patch size.

5. MEASUREMENT RESULTS

The simulated antenna was fabricated and tested. Figure 11 shows the antenna being tested on the network analyzer. The radiation pattern of the antenna was measured in an anechoic chamber. Figures 12 through 15 show the simulated and measured radiation patterns of the antenna in both the E-plane and the H-plane at the frequency bands of 2.4 GHz and 5.8 GHz. The simulated and measured radiation patterns in the following Figures 12 through 15 have been normalized so that the maxima are set to 0 dB. Good agreement is found between the simulated and measured values except in Figure 15. This may be due to the fact that very low power levels are received by the antenna at 5.8 GHz band in H-plane configuration as compared to the other 3 configurations (Figures 12–14) so the measurement apparatus might be

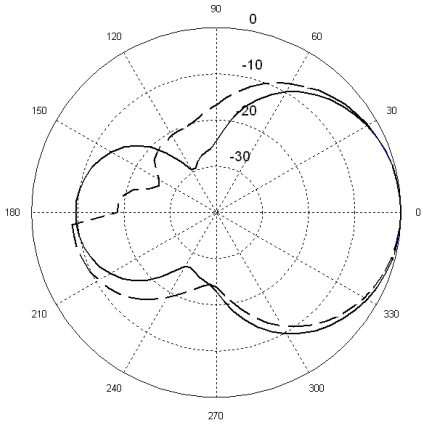

Figure 12. Simulated (solid) and Measured (dash) *E*-plane radiation pattern at 2.4 GHz.

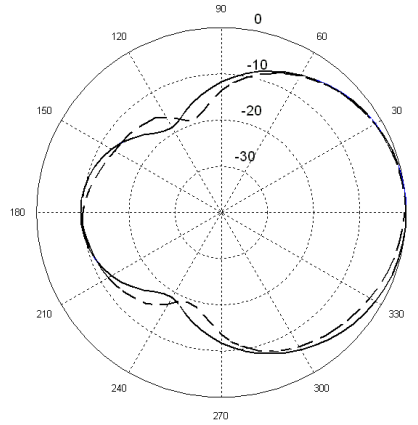

Figure 13. Simulated (solid) and Measured (dash) *H*-plane radiation pattern at 2.4 GHz.

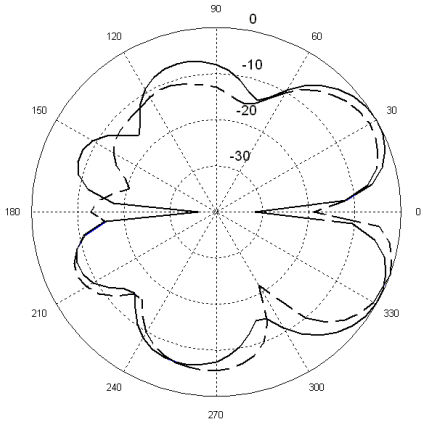

Figure 14. Simulated (solid) and Measured (dash) *E*-plane radiation pattern at 5.8 GHz.

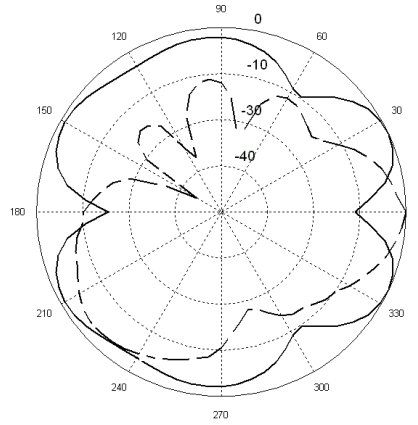

Figure 15. Simulated (solid) and Measured (dash) H-plane radiation pattern at 5.8 GHz.

unable to verify the simulation result for this particular configuration (*H*-plane at 5.8 GHz) due to possible presence of interference and noise.

The simulated and measured gain curves are also given for the 2.4 GHz and 5.8 GHz bands in Figure 16. At the 2.4 GHz band the maximum power was received by the antenna at the broadside direction while at the 5.8 GHz band the maximum power was received at an angle

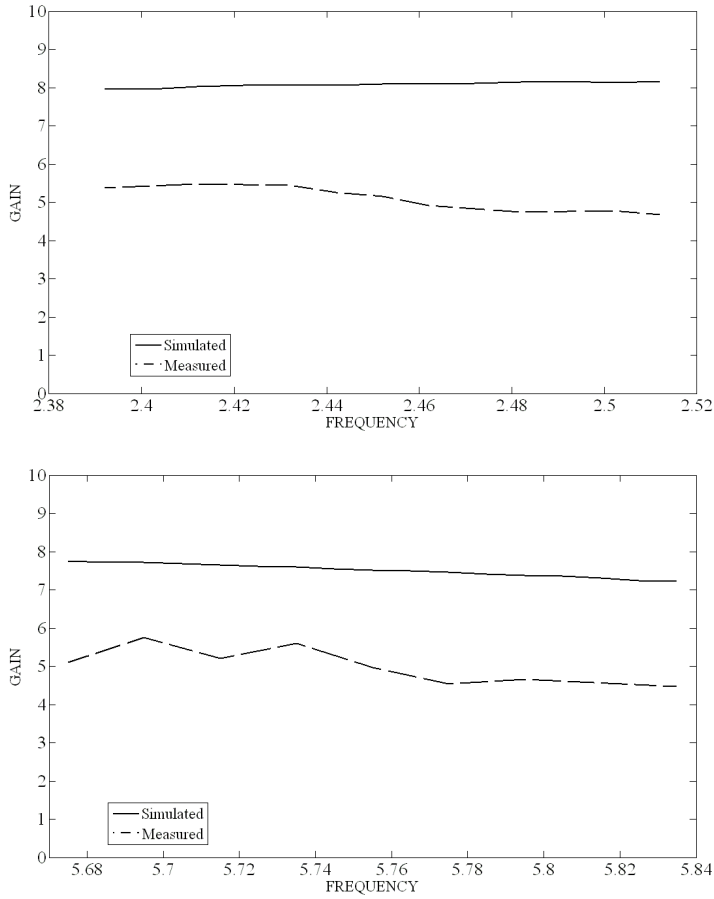

Figure 16. Simulated (solid) and Measured (dash) Gains at the 2.4 GHz and 5.8 GHz bands.

of 30° with respect to broadside in the E-plane. Consequently, gain measurements are done for the two frequency bands in the directions of their respective maxima using the substitution/gain-transfer technique with the help of a standard horn antenna with calibrated gain. About 2–3 dB of difference in the simulated and measured gains is observed which can be attributed to fabrication and measurement errors.

6. CONCLUSIONS

A novel stacked microstrip patch antenna was designed with fractal shaped defects being excoriated from both the patch surfaces. It

resulted in longer current paths on the patches which led to a size reduction of roughly 67% for both the patches in comparison with a stacked U-slot antenna which was previously designed by the authors. In addition the use of a stacked patch resulted in additional design parameters which were used to optimize the dual band performance of the antenna. The return loss of the antenna indicates a −10 dB impedance bandwidth of 120 MHz at the 2.4 GHz band and an impedance bandwidth of 160 MHz at the 5.8 GHz band.

REFERENCES

1. Lo, T. K. and Y. Hwang, "Microstrip antennas of very high permittivity for personal communications," *1997 Asia Pacific Microwave Conference*, 253–256, 1997.
2. Sinati, R. A., *CAD of Microstrip Antennas for Wireless Applications*, Artech House, Norwood, MA, 1996.
3. Wang, H. Y. and M. J. Lancaster, "Aperture-coupled thin film superconducting meander antennas," *IEEE Transaction on Antennas and Propagation*, Vol. 47, 829–836, 1999.
4. Waterhouse, R., *Printed Antennas for Wireless Communications*, John Wiley & Sons Inc, 2007.
5. Anguera, J., L. Boada, C. Puente, C. Borja, and J. Soler, "Stacked H-shaped microstrip patch antenna," *IEEE Transactions on Antennas and Propogation*, Vol. 52, No. 4, April 2004.
6. Kordzadeh, A. and F. Hojat Kashani, "A new reduced size microstrip patch antenna with fractal shaped defects," *Progress In Electromagnetics Research B*, Vol. 11, 29–37, 2009.
7. Sanad, M. and N. Hassan, "Mobile cellular/GPS/satellite antennas with both single-band and dual-band feed points," *Proc. IEEE Antennas and Propagation Int. Symp.*, Vol. 1, 298–301, Salt Lake City, UT, July 2000.
8. Moleiro, A., J. Rosa, R. Nunes, and C. Peixeiro, "Dual band microstrip patch antenna element with parasitic for GSM," *Proc. IEEE Antennas and Propagation Int. Symp.*, Vol. 4, 2188–2191, Salt Lake City, UT, July 2000.
9. Zhong, S. S. and J. H. Cui, "Compact dual-frequency microstrip antenna," *Proc. IEEE Antennas and Propagation Int. Symp.*, Vol. 4, 2196–2199, Salt Lake City, UT, July 2000.
10. Tiwari, H. and M. V. Kartikeyan, "Design studies of stacked U-slot microstrip patch antenna for dual band operation," *35th International Conference on Infrared, Millimeter and Terahertz Waves*, 2010 (Accepted).